DOI: 10.13009/EUCASS2017-263

Sector demand analysis under meteorological uncertainty

Alfonso Valenzuela, Antonio Franco and Damián Rivas,
Department of Aerospace Engineering
Escuela Técnica Superior de Ingeniería, Universidad de Sevilla
41092 Sevilla, Spain

Abstract

In this paper, a methodology to assess the uncertainty of sector demand when subject to weather uncertainty is presented. The methodology requires the definition of a scenario (in terms of Air Traffic Control sector, flights, and weather forecasts to be considered), the processing of meteorological data (provided by Ensemble Prediction Systems, which are composed of different possible atmosphere realizations), and a trajectory predictor (which, for each flight and for each atmosphere realization, computes a different aircraft trajectory). The computed trajectories, along with the information of the sector, are then used to analyse the sector demand, which is described in terms of entry count (number of flights entering the sector during a selected time period). The analysis is based on the statistical characterization of the entry times of the flights to the sector and of the entry count. The probability of the entry count exceeding the declared capacity of the sector is obtained. A realistic application example is provided to show the potentiality of the methodology.

1. Introduction

In 2005, the European Commission stated the political vision and high level goals for the Single European Sky and its technological pillar SESAR. Accomplishing the goals of increasing capacity and improving safety requires a paradigm shift in operations through state-of-the-art, innovative technology and research. A promising approach that can improve current prediction and optimization mechanisms towards meeting these goals is to model, analyse, and manage the uncertainty present in Air Traffic Management (ATM).

Weather uncertainty is one of the main sources of uncertainty that affect the ATM system, as identified by the ComplexWorld Research Network [1]. The limited knowledge about present and, especially, future meteorology conditions, such as wind velocity and direction, fog, snowfall or storms, is responsible for much of the delays and flight cancellations, which negatively affects ATM efficiency and translates to extra costs for airlines and air navigation service providers.

The work presented in this paper aims to understand how weather uncertainty is propagated from the trajectory scale to the traffic scale and, in particular, to quantify the effects of this uncertainty on the demand of an Air Traffic Control (ATC) sector. The general framework of this work is the project TBO-Met[1], funded by the SESAR Joint Undertaking. The overall objective of this project is threefold: 1) to advance in the understanding of the effects of meteorological uncertainty in Trajectory-Based Operations (TBO), 2) to develop methodologies to quantify and reduce the effects of meteorological uncertainty in TBO, and 3) to pave the road for a future integration of the management of meteorological uncertainty into the ATM system.

Ensemble Weather Forecasting is a prediction technique that allows to estimate the uncertainty in a weather forecast. In this work, the meteorological uncertainty is provided by Ensemble Prediction Systems (EPS). Typically, an EPS is a collection of 10 to 50 forecasts, referred to as members, with forecasting horizons of up to 2-5 days. They consist on running many times a deterministic model from very slightly different initial conditions [2]. Often, the model physics is also slightly perturbed, and some ensembles use more than one model within the ensemble or the same model but with different combinations of physical parameterization schemes. This technique generates a representative sample of the possible realizations of the potential weather outcome. The uncertainty information is on the spread of the

[1] https://tbomet-h2020.com/

DOI: 10.13009/EUCASS2017-263

solutions in the ensemble, and the hope is that the spread of the predictions in the ensemble brackets the true weather outcome [3].

Uncertain trajectories are obtained during the process of trajectory planning when meteorological uncertainty is taken into account. For each flight, a trajectory predictor computes an ensemble of aircraft trajectories, each one corresponding to a different member of the EPS [4]. Because they are computed for different weather realizations, different flight durations and fuel consumptions are obtained [5,6]. These trajectories, along with the information of the ATC sector, are then used to analyse the sector demand.

In this work, the sector demand is described in terms of the entry count, which is defined as the number of flights entering the ATC sector during a selected time period [7]. This count is obtained from the intersections of the individual aircraft trajectories with the geometry of the sector. Since the aircraft trajectories are uncertain, then the associated entry times are also uncertain and, thus, the entry count is also uncertain. The analysis is then based on the statistical characterization of these times and this count.

2. Methodology

The general scheme for the analysis of sector demand is shown in Figure 1. Initially, the scenarios have to be defined, in terms of: 1) ATC sector (e.g., geometry and capacity), 2) flights that cross the sector (e.g., origin and destination, route, departure time, flight levels, and cruise speeds), and 3) weather forecast (e.g., EPS to be considered, release time, and forecast times).

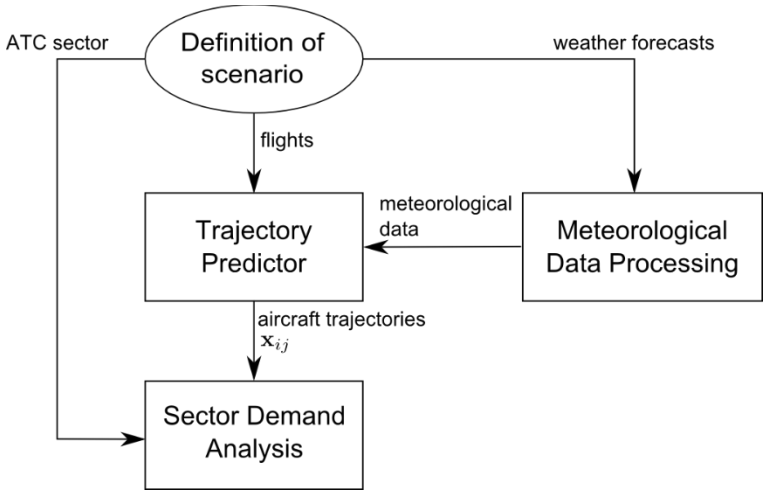

Figure 1: General scheme for the analysis of sector demand

The meteorological data provided by the weather forecasts are then processed for its use by the trajectory predictor. For example, the necessary values of wind and air temperature are extracted, and information about convection can derived from different parameters.

The trajectory predictor computes, for each flight and for each weather prediction, a different aircraft trajectory. The trajectory predictor specifically developed for the application considered in this paper is described in Section 3.

The computed trajectories, along with the information of the ATC sector, are then used to perform the analysis of the sector demand. The different atmospheric realizations lead to different predicted entry times and, therefore, to different entry counts.

To perform the analysis of the sector demand, the entry times of the flights to the sector and the entry count are statistically characterized. Mean, maximum, and minimum values, and the spread of the times and of the count, measured as the difference between the maximum and minimum values, are examined. The analysis allows to determine which flights contribute the most to the demand uncertainty. The probability of the entry count exceeding a

DOI: 10.13009/EUCASS2017-263

given threshold is also obtained, which can be used to represent the probability that the demand exceeds the capacity of the ATC sector.

Next, some definitions are provided and the general hypotheses are established. Following, the entry time and the entry distance are described, obtained from the individual aircraft trajectories. Finally, the entry count is also described, obtained from the entry times.

2.1 Definitions and general hypotheses

In this work, it is considered that the geometry of the ATC sector is fixed and does not change with time. Therefore, the effects of opening/closing sectors are not analysed.

It is considered that there exist m different flights and that the EPS is formed by n different members or atmospheric realizations. The position of flight i ($i = 1, \dots, m$) for member j ($j = 1, \dots, n$) at time t, is denoted as $\mathbf{x}_{ij}(t)$. It is given by the longitude λ, the latitude ϕ, and the pressure altitude h:

$$\mathbf{x}_{ij}(t) = \left[\lambda_{ij}(t), \phi_{ij}(t), h_{ij}(t)\right]. \tag{1}$$

The trajectories $\mathbf{x}_{ij}$ generated by the trajectory predictor are provided as a list of discrete points and times. A linear interpolation is used to obtain the position of the flight at any time.

In this work, it is considered that the trajectory crosses the ATC sector only once; trajectories crossing the same sector multiple times are not considered (for example, flights that return to the departure airport) since this is an uncommon practice in commercial aviation.

2.2 Entry time and entry distance

If the trajectory $\mathbf{x}_{ij}$ crosses the ATC sector, then there exist an entry time to the sector $t_{ij,E}$ and the associated entry point $\mathbf{x}_{ij}\left(t_{ij,E}\right)$. The uncertainty information is on the spread of these times.

The entry times are statistically characterized. For flight i, we define the average entry time $t_{i,E}$ as

$$t_{i,E} = \frac{1}{n}\sum_{j=1}^{n} t_{ij,E}, \tag{2}$$

The dispersion of the entry times for flight i, $\Delta t_{i,E}$, is defined as the difference between the maximum and the minimum values for the different atmospheric realizations

$$\Delta t_{i,E} = \max_j t_{ij,E} - \min_j t_{ij,E}, \tag{3}$$

For flight i and for ensemble member j, the entry distance is the distance travelled by the aircraft from its origin to the entry point, denoted as $d_{ij,E}$. Since the trajectories will be provided as a list of discrete points, the distance between two consecutive points is calculated considering a rhumb line (see, for example, Section 3).

The entry distance are also statistically characterized. The average value and the dispersion are defined as follows

$$d_{i,E} = \frac{1}{n}\sum_{j=1}^{n} d_{ij,E}, \tag{4}$$

$$\Delta d_{i,E} = \max_j d_{ij,E} - \min_j d_{ij,E}, \tag{5}$$

If it happens that for a particular member the trajectory does not cross the sector, then the entry time and the entry distance are not defined, and as consequence, this member is not considered for the computation of the mean and the dispersion values.

DOI: 10.13009/EUCASS2017-263

2.3 Entry count

The entry count for a given sector is defined as the number of flights entering the sector during a selected time period P_k,

$$P_k = [kt_s, kt_s + \delta t), \qquad k = 0,1,2,\ldots \tag{6}$$

where t_s is a step value that defines the time difference between the start times of two consecutive time periods, and δt is the duration of each time period. To clarify this definition, in Figure 2 a deterministic example of the entry (E) and exit (X) times of eight flights, and four time periods, with $\delta t = 2t_s$, is given. In this example, it is obtained that the entry count is 3 flights for period P_0 (flights 3, 4, and 5), 3 flights for period P_1 (flights 4, 5, and 6), 3 flights for period P_2 (flights 6, 7, and 8), and 2 flights for period P_3 (flights 7 and 8).

Because the entry time is uncertain, the aircraft may enter the sector in different time periods, thus leading to an uncertain entry count. The larger the dispersion of the entry time and the smaller the values of t_s and δt, the more likely the entry count to be uncertain. For example, in case that the dispersion of the entry time of one flight is larger than the duration of the time period, then this flight may enter the sector in two or more consecutive time periods.

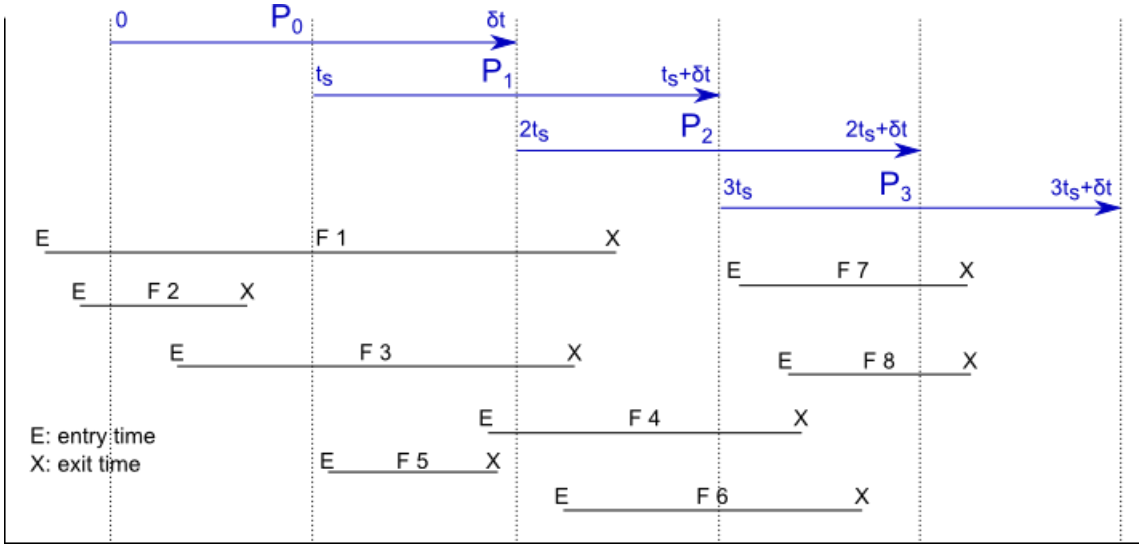

Figure 2: Example of entry and exit times for eight flights, and four time periods with $\delta t = 2t_s$. Adapted from [7].

We define an entry function for flight i, for ensemble member j, and for time period P_k, denoted as $E_{ij}(P_k)$. It takes the value 1 when the aircraft enters the ATC sector during this time period and the value 0 otherwise

$$E_{ij}(P_k) = \begin{cases} 1, & \text{if } t_{ij,E} \in P_k, \\ 0, & \text{otherwise.} \end{cases} \tag{7}$$

The entry count for ensemble member j and for time period P_k, denoted as $E_j(P_k)$, is obtained as the sum of the entries of the different flights

$$E_j(P_k) = \sum_{i=1}^{m} E_{ij}(P_k). \tag{8}$$

From these n values of the entry count, mean, maximum, and minimum values ($\bar{E}$, E_{max}, and E_{min}, respectively) for time period P_k are determined

$$\bar{E}(P_k) = \frac{1}{n}\sum_{j=1}^{n} E_j(P_k), \tag{9}$$

$$E_{max}(P_k) = \max_j E_j(P_k), \tag{10}$$

$$E_{min}(P_k) = \min_j E_j(P_k). \tag{11}$$

The uncertainty information is on the spread of the entry count. The dispersion of the entry count, $\Delta E(P_k)$, is defined as follows

DOI: 10.13009/EUCASS2017-263

$$\Delta E(P_k) = E_{max}(P_k) - E_{min}(P_k). \tag{12}$$

The probability of the entry count E being greater than a given value a for time period P_k , e.g. the declared capacity, is obtained from the number of entry counts $E_j(P_k)$ that are greater than this value, as follows

$$P[E(P_k) > a] = \frac{\text{number of } E_j(P_k) > a}{n}. \tag{13}$$

Notice that, since the entry of each flight to the ATC sector for time period P_k only depends on the entry time $t_{ij,E}$, see Eq. (7), then the entry count and its statistical characterization are only affected by the uncertainty in this time. For one particular flight, the uncertainty in the entry time is expected to increase due to meteorological reasons when:

- the forecasting horizon increases,
- the aircraft flies over regions with high uncertainty before entering the sector, and
- the aircraft travels a large distance before entering the sector, thus accumulating uncertainty along the flight.

Correspondingly, the uncertainty in the entry count is expected to increase when:

- the entry count is computed far in advance,
- the aircraft are affected by meteorological phenomena with large uncertainty before entering the sector, and
- the traffic is composed of many flights arriving from distant locations.

3. Application

In this section, an application example is provided to show the potentiality of the presented methodology. In this application, the demand of an ATC sector is analysed for a whole day (from 00:00 to 24:00) when predicted the day before (at 00:00). Firstly, in Section 3.1, the traffic scenario is described, in terms of ATC sector, flights, and weather forecasts to be considered. In Section 3.2, the trajectory predictor developed for this application is described. The results are presented and analysed in Section 4.

3.1 Traffic scenario

ATC sector

The ATC sector LECMSAU, located in the Northwest of Spain, see Figure 3, is considered in this application. It ranges from FL 345 to FL 460, and the coordinates of the vertices that define the lateral boundary have been obtained from Eurocontrol's Network Strategic Tool (NEST) for the Aeronautical Information Regulation and Control (AIRAC) cycle 1701. The declared capacity of this sector (i.e., the maximum number of flights entering the sector per hour) is 36 flights/hour, also obtained from NEST and AIRAC cycle 1701.

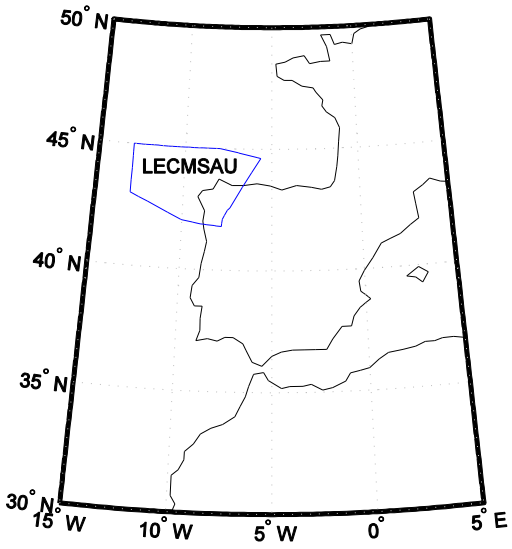

Figure 3. Geographical location of ATC sector LECMSAU.

DOI: 10.13009/EUCASS2017-263

Flights

In this application, the traffic that planned to cross this sector between 00:00 and 24:00 on 07 January 2017 is analysed. This traffic is retrieved from NEST software (AIRAC cycle 1701), and it corresponds to the last filed flight plan from the airlines (i.e., initial trajectories, according to NEST nomenclature). It is considered that each flight has a fixed route, provided by its flight plan, the same for all EPS members. For simplicity, it is considered that the trajectories are flown at constant pressure altitude for the whole flight (from origin to destination).

A total number of 468 flights is obtained from NEST for this date and ATC sector. However, four of these flights are discarded, those flights arriving or departing to/from LEST airport (Santiago de Compostela). The reason is that, under the hypothesis of flying at constant pressure altitude, these flights instantly appear or disappear inside the sector, not crossing the sector boundaries. Thus, a total number of 464 flights is considered in this application.

The routes followed by the 464 flights, defined by the coordinates of their waypoints, are shown in Figure 4. They are represented from the departure airports to the exit points of the sector (since the routes from the exit points to the arrival airports are not of interest in this analysis, they are not represented). This traffic is composed of short flights (departing from Portugal, Spain, and France), medium flights (mainly flights from the Canary Islands, the British Isles, and the Scandinavian Peninsula), and long flights (from America).

The relative frequency of the distance between the departure airport and the entry point is shown in Figure 5. Approximately, 9% of the flights travel less than 500 km before entering the sector, 26% between 500 and 1000 km, 21% between 1000 and 1500 km, 31% between 1500 and 2000 km, and 13% more than 2000 km. This represents an equilibrated mix of flights with different distances.

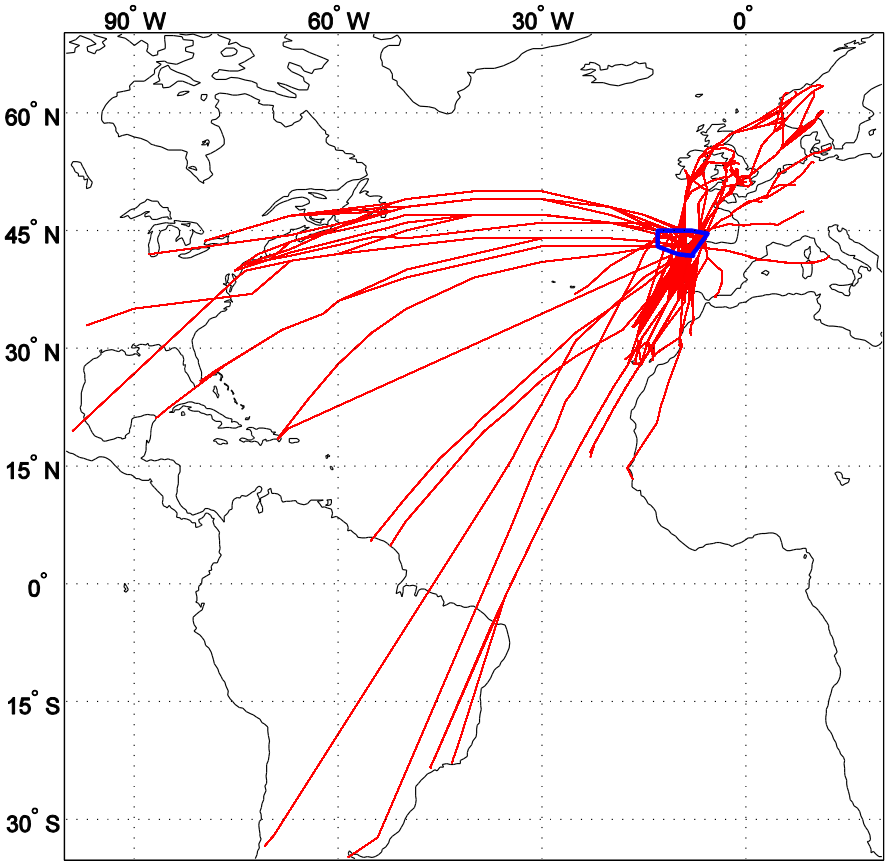

Figure 4. Traffic crossing LECMSAU on 07 January 2017 according to flight plans.

The trajectory predictor described in Section 3.2 requires the following information for each flight:

- departure time: obtained from NEST;
- coordinates of the waypoints that define the route: obtained from NEST;

DOI: 10.13009/EUCASS2017-263

- pressure altitude: fixed to 200 hPa (approximately 38600 ft) for all aircraft and the whole flight;
- airspeed: the average cruise Mach provided by Eurocontrol's Base of Aircraft Data (BADA) 3.13 [8] for the aircraft model that performs the flight is considered for the whole flight (from origin to destination), ranging from 0.70 to 0.85.

Weather forecast

In this application, the meteorological uncertainty is retrieved from the European Centre for Medium-Range Weather Forecasts. In particular, the weather forecast ECMWF-EPS, composed of 51 members, is used. It is considered that the analysis is performed the day before the operation; thus, the forecasts released at 00:00 on 06 January 2017 are considered.

According to the flight plans retrieved from NEST, the earliest flight departs at 17:25 on 06 January and, as a reference, the latest flight arrives to its destination at 04:00 on 08 January. Taking into account these times, the forecasts with time steps of 12, 18, 24, 30, 36, 42, 48, and 54 hours are considered in this application.

In agreement with the coordinates of the route waypoints, the forecasts are retrieved for a coverage area which ranges from 35 degrees South to 70 degrees North, and from 100 degrees West to 55 degrees East. The spatial grid resolution is 0.25 degrees. According to the cruise altitude chosen for all flights, the forecasts are retrieved for the pressure level 200 hPa.

The meteorological variables required by the trajectory predictor described in Section 3.2 are the zonal and the meridional winds (winds along the West-East and South-North directions, respectively), and the air temperature.

In Figures 5 to 7, the average and dispersion of the meridional wind, the zonal wind, and the air temperature are shown for the forecast corresponding to the time instant 12:00 on 07 January. The dispersion is measured as the difference between the maximum and the minimum values at each geographic location. Notice that, since the entry count is affected by the uncertainty the flights encounter before entering the sector (see Section 2), the area represented in these figures is the same area represented in Figure 4, which covers the trajectories of the flights that enter LECMSAU.

The average meridional wind, see Figure 5 left, ranges approximately between -30 m/s (South direction) and 40 m/s (North direction). High values of the wind are found at the East coast of North America, and a high variation (approximately 70 m/s) is found between the Canary Islands and the Azores. The average zonal wind, see Figure 5 right, is larger than the meridional wind, ranging approximately between -20 m/s (West direction) and 70 m/s (East direction). The zonal wind is therefore the main contributor to the existence of jet streams. The larger values are found again at the East coast of North America, and at the Northwest of Africa.

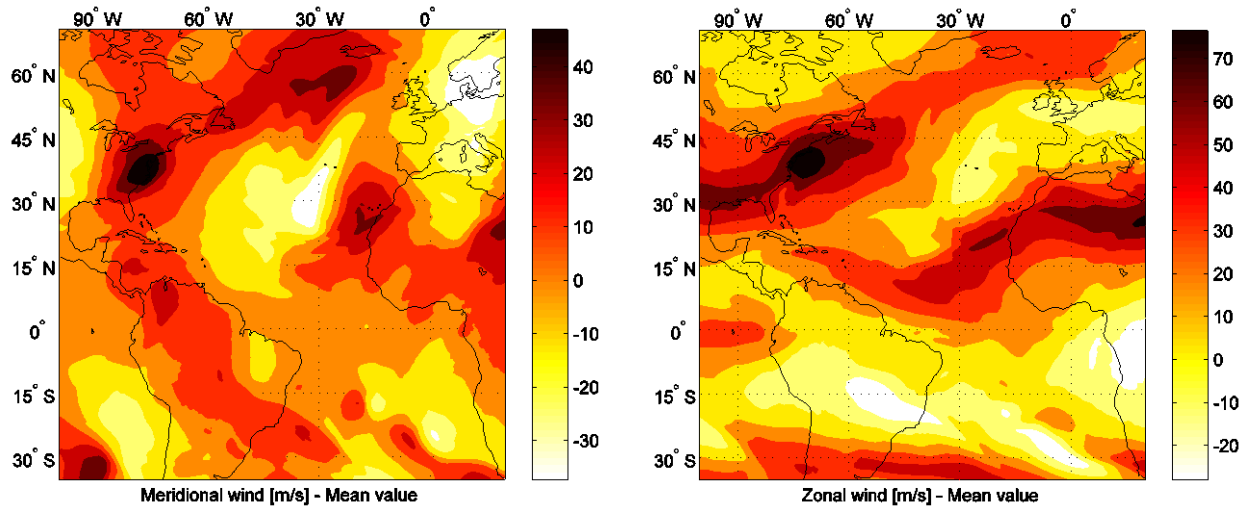

Figure 5. Average meridional (left) and zonal (right) winds, ECMWF-EPS released at 00:00, 06/01/17, step 36 hours.

The dispersion of the meridional and zonal winds is shown in Figure 6, respectively. In both cases, the dispersion can be rather large, with maximum values above 40 m/s. The geographic areas affected by high uncertainty are

DOI: 10.13009/EUCASS2017-263

approximately the same in both cases. In particular, the following regions can be highlighted: 1) the East coast of North America and the North Atlantic, affecting flights from North America to Europe, and 2) South America and the Atlantic Ocean near the Equator, affecting flights from South America to Europe.

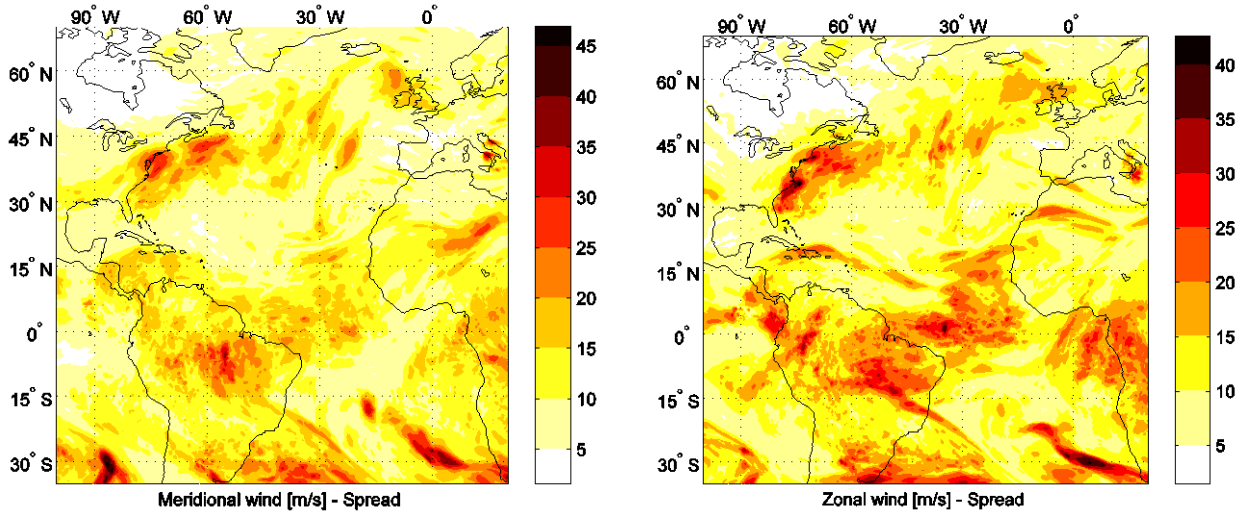

Figure 6. Dispersion of the meridional (left) and zonal (right) winds, ECMWF-EPS released at 00:00, 06/01/17, step 36 hours.

The average air temperature is presented in Figure 7 left. It can be seen that there is a cold area at the North Atlantic (approximately -65 ˚C), and a hot area very close to it, at the Labrador Peninsula and Greenland (approximately -45 ˚C). The dispersion at the North Atlantic is approximately 10 ˚C, see Figure 7 right.

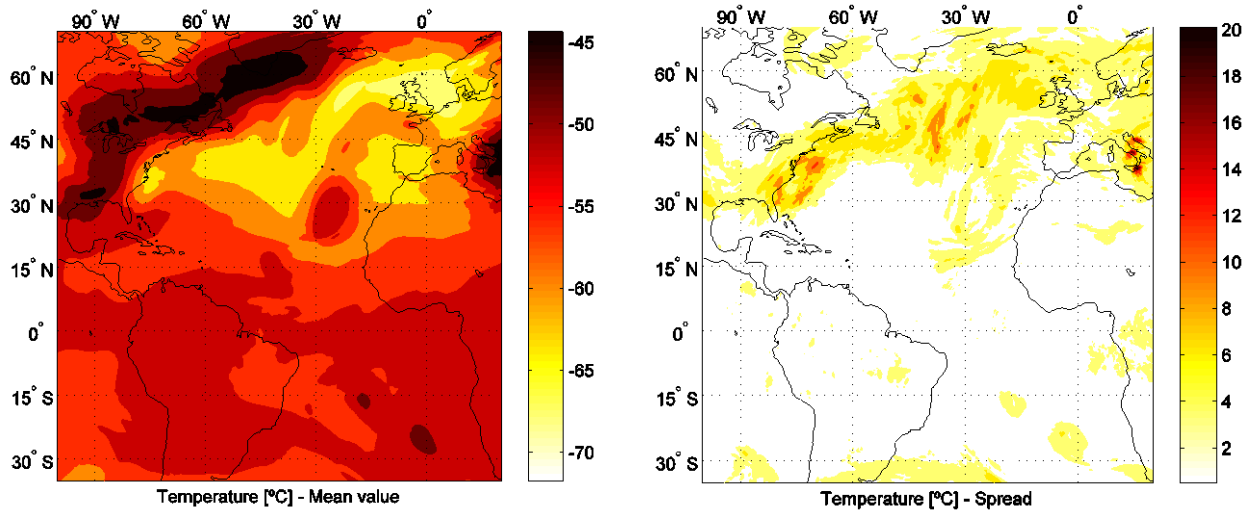

Figure 7. Average value (left) and dispersion (right) of the air temperature, ECMWF-EPS released at 00:00, 06/01/17, step 36 hours.

3.2 Trajectory predictor

As indicated in Section 2, the trajectory predictor determines the aircraft trajectory for each flight and for each possible atmospheric scenario. As the coordinates of the waypoints defining the route of each flight are given, the objective of the trajectory predictor is to provide, for each flight and for each forecast member, a list of discrete times: the estimated times over the waypoints when variable horizontal winds and variable air temperature are encountered.

In this application a Spherical Earth is considered, with mean radius $R_E = 6371$ km.

DOI: 10.13009/EUCASS2017-263

Characterization of the routes

A trajectory is considered to be composed of several cruise segments connecting the given waypoints that define the route. Each one of these segments is defined by a constant course, and is flown at constant Mach number and constant pressure altitude.

For flight i ($i = 1, \dots, m$) and for segment k ($k = 1, \dots, p_i$, where p_i is the number of segments of the route), the longitude and latitude of the waypoints that define the segment are denoted as $\lambda_i^{[k-1]}$, $\lambda_i^{[k]}$, $\phi_i^{[k-1]}$ and $\phi_i^{[k]}$, respectively. For segment k, the course $\psi_i^{[k]}$ and the segment length $l_i^{[k]}$ can be computed from the following navigation equations:

$$\tan\psi_i^{[k]} = \frac{\lambda_i^{[k]} - \lambda_i^{[k-1]}}{\ln\left[\frac{\tan\left(\pi/4 - \phi_i^{[k-1]}/2\right)}{\tan\left(\pi/4 - \phi_i^{[k]}/2\right)}\right]} \tag{14}$$

$$l_i^{[k]} = \begin{cases} \dfrac{R_E\left(\phi_i^{[k]} - \phi_i^{[k-1]}\right)}{\cos\psi_i^{[k]}}, & \text{if } \phi_i^{[k]} \neq \phi_i^{[k-1]}, \\ R_E\cos\phi_i^{[k-1]}\left|\lambda_i^{[k]} - \lambda_i^{[k-1]}\right|, & \text{if } \phi_i^{[k]} = \phi_i^{[k-1]}, \end{cases} \tag{15}$$

where it has been assumed that the 180th meridian is never crossed. Note that, if $\phi_i^{[k]} = \phi_i^{[k-1]}$, Eq. (31) becomes $\psi_i^{[k]} = \mathrm{sgn}\left(\lambda_i^{[k]} - \lambda_i^{[k-1]}\right)\frac{\pi}{2}$.

Taking the accumulated distance travelled over the Earth along the trajectory, r, as the independent variable, one can obtain the position of flight i at distance r, that is, the vector $\mathbf{x}_i(r) = [\lambda_i(r), \phi_i(r), h_i]$, from the equations of navigation along constant rhumb lines:

$$\phi_i(r) = \phi_i^{[k-1]} + \frac{r - r_i^{[k-1]}}{R_E}\cos\psi_i^{[k]}, \quad \text{if } r \in \left[r_i^{[k-1]}, r_i^{[k]}\right], \tag{16}$$

$$\lambda_i(r) = \begin{cases} \lambda_i^{[k-1]} + \tan\psi_i^{[k]}\ln\left[\dfrac{\tan\left(\frac{\pi}{4} - \frac{\phi_i^{[k-1]}}{2}\right)}{\tan\left(\frac{\pi}{4} - \frac{\phi_i(r)}{2}\right)}\right], & \text{if } \phi_i(r) \neq \phi_i^{[k-1]} \text{ and } r \in \left[r_i^{[k-1]}, r_i^{[k]}\right], \\ \lambda_i^{[k-1]} + \dfrac{l_i^{[k]}\,\mathrm{sgn}\left(\lambda_i^{[k]} - \lambda_i^{[k-1]}\right)}{R_E\cos\phi_i^{[k-1]}}, & \text{if } \phi_i(r) = \phi_i^{[k-1]} \text{ and } r \in \left[r_i^{[k-1]}, r_i^{[k]}\right], \end{cases} \tag{17}$$

where $r_i^{[k]}$ is the accumulated distance corresponding to the kth waypoint, given by $r_i^{[k]} = \sum_{q=1}^{k} l_i^{[q]}$ (for $k = 1, \dots, p_i$) and $r_i^{[0]} = 0$.

Atmospheric variables along the route

The flights are supposed to be subject to variable meridional and zonal winds (horizontal winds), and variable air temperature. For member j ($j = 1, \dots, n$), these atmospheric variables are considered to be location and time dependent, and are denoted by $w_{m,j}(\lambda, \phi, h, t)$, $w_{z,j}(\lambda, \phi, h, t)$ and $T_j(\lambda, \phi, h, t)$, respectively. Linear interpolation is performed to obtain meridional and zonal winds and air temperature for a specific location and time (i.e. for a given query point) from gridded values provided by the retrieved weather forecast.

Taking into account Eqs. (16-17), for flight i and for member j, one has:

$$w_{m,ij}(r,t) = w_{m,j}[\lambda_i(r), \phi_i(r), h_i, t], \tag{18}$$

$$w_{z,ij}(r,t) = w_{z,j}[\lambda_i(r), \phi_i(r), h_i, t], \tag{19}$$

$$T_{ij}(r,t) = T_j[\lambda_i(r), \phi_i(r), h_i, t]. \tag{20}$$

Furthermore, meridional and zonal winds can be transformed into along-track winds and crosswinds by a rotation of axes:

DOI: 10.13009/EUCASS2017-263

$$\begin{bmatrix} w_{ij}(r,t) \\ w_{c,ij}(r,t) \end{bmatrix} = \begin{bmatrix} \cos\psi_i^{[k]} & \sin\psi_i^{[k]} \\ -\sin\psi_i^{[k]} & \cos\psi_i^{[k]} \end{bmatrix} \begin{bmatrix} w_{m,ij}(r,t) \\ w_{z,ij}(r,t) \end{bmatrix}, \qquad \text{for } r \in \left[r_i^{[k-1]}, r_i^{[k]}\right]. \tag{21}$$

Note that the along-track wind is positive for tailwinds and the crosswind is positive if it blows from the left wing.

Kinematic equation of motion

The effects of the crosswinds are considered in a simplified manner, taking them into account in the kinematic equations, ignoring the lateral dynamics, and translating the crosswind into an equivalent headwind. This leads to a reduced ground speed for flight i and for member j, which is given by

$$V_{g,ij}(r,t) = \sqrt{\gamma R_g T_{ij}(r,t) M_i^2 - w_{c,ij}^2(r,t)} + w_{ij}(r,t). \tag{22}$$

where M_i is the constant Mach number for flight i, γ is the ratio of specific heats of the air and R_g is the gas constant of the air.

Finally, for flight i and for member j, the estimated times over the waypoints, namely $t_{ij}^{[k]}$ $(k = 0, \dots, p_i)$, can be determined by first solving the following initial value problem,

$$\begin{cases} \dfrac{dt_{ij}}{dr} = \dfrac{\left(1 + \dfrac{h_i}{R_E}\right)}{V_{g,ij}(r, t_{ij})} \\ t_{ij}(0) = t_i^{[0]} \end{cases} \tag{23}$$

where $t_i^{[0]}$ is the given departure time, and then evaluating at the accumulated distances corresponding to the waypoints: $t_{ij}^{[k]} = t_{ij}\left(r_i^{[k]}\right)$, for $k = 1, \dots, p_i$. Note that $t_{ij}^{[0]} = t_i^{[0]}$ for any forecast member.

4. Results

This section is organised as follows. First, the entry times are analysed. Next, the entry count is presented for two different values of the step t_s and of the duration of the time period δt. Finally, the probability of exceeding the declared capacity of the sector is also presented for two different values of t_s and of δt.

Entry times

The dispersion of the entry time, $\Delta t_{i,E}$, as a function of the distance to the entry point, $d_{i,E}$, for each flight is presented in Figure 8 (notice that, since in this application the route of each flight is the same for all the atmospheric realizations, then the distance $d_{ij,E}$ is the same for all the ensemble members). As expected, the dispersion increases as the distance increases because the uncertainty is accumulated along the trajectories; flights arriving from distant locations present more uncertainty. The maximum value of the dispersion is 584 seconds, whereas the minimum value is 6 seconds.

It can be seen that there are flights with similar distances but different values of dispersion. For example, for $d_{i,E}$ approximately equal to 2000 km, the dispersion ranges between 119 and 206 seconds. As possible causes of these different values, the following ones can be highlighted:

- different routes (flights over regions of the airspace with different uncertainty),
- different effects of the same wind uncertainty on different flights (uncertainties in tail/headwinds have a higher impact than uncertainties in crosswinds),
- different departure times (the predictions for flights departing later are made with weather forecasts with larger time horizons, thus having a larger uncertainty), or
- different speeds (flights with lower values of Mach number and with headwinds are more sensitive to uncertainties in the wind, and flights with higher values of Mach number are more sensitive to uncertainties in the air temperature).

The relative frequency of the dispersion of the entry time is shown in Figure 9. In this application, 13% of the flights have a dispersion below 1 minute, 29% between 1 and 2 minutes, 39% between 2 and 3 minutes, 14% between 3 and 4 minutes, and 5% above 4 minutes.

DOI: 10.13009/EUCASS2017-263

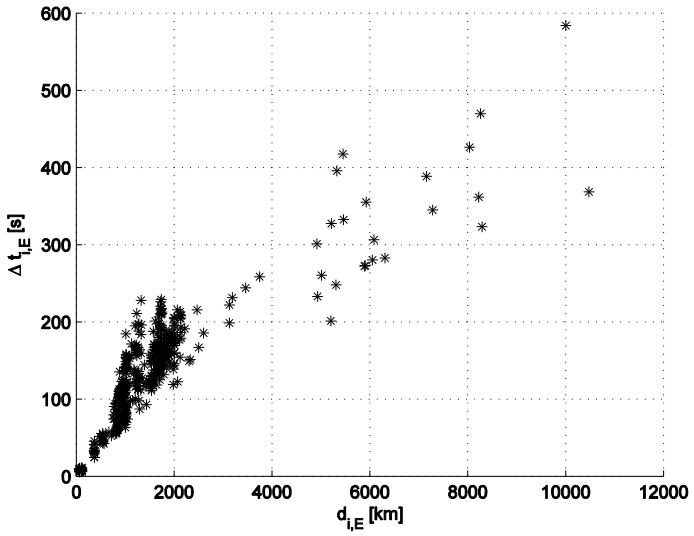

Figure 8. Dispersion of the entry time vs distance to the entry point.

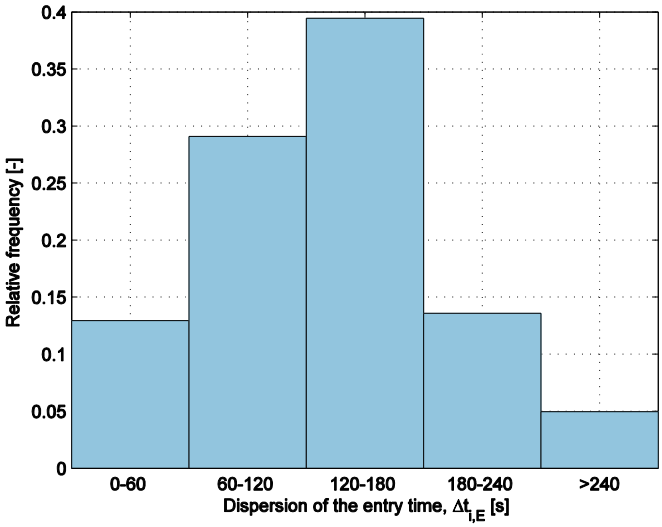

Figure 9. Relative frequency of the dispersion of the entry time.

Entry count

The maximum, average, and minimum values of the entry count for t_s =60 min and δt =60 min are shown in Figure 10 (for each time interval, these figures display three superposed vertical bars: the minimum, mean, and maximum values of the entry count). The largest value of the mean entry count is 44.0 flights (for the time period 14:00-15:00).

The uncertainty on this count is on the spread of the number of flights. The difference between the maximum and the minimum values of the entry count is as large as 3 flights (for 15:00-16:00, 21:00-22:00, and 22:00-23:00). The dispersion of the entry count is shown in Figure 11. From this figure it can be observed that the dispersion is 3 flights for a total of 3 hours (in disjoint periods), 2 flights for 6 hours, 1 flight for 6 hours, and 0 flights for the remaining 9 hours. For the occupancy count, the dispersion is 3 flights for 2 hours, 2 flights for 7 hours, 1 flight for 6 hours, and 0 flights for the remaining 9 hours.

It is worth noting that, in this application, where only wind and air temperature uncertainties are considered, these uncertainties are rather large when compared, for example with the declared capacity; 3 flights compared with 36

DOI: 10.13009/EUCASS2017-263

flights/hour is about 8%. One would expect to obtain even larger values of uncertainty in scenarios that consider uncertainties on convective phenomena.

Taking into account that the declared capacity is 36 flights/hour (represented as a red line along with the entry count in Figure 10), this capacity is exceeded for time periods 08:00-09:00, 14:00-15:00, 16:00-17:00. In fact, according to NEST, an ATFCM regulation was activated (named SAU07) in the period 14:00-16:11 due to ATC capacity.

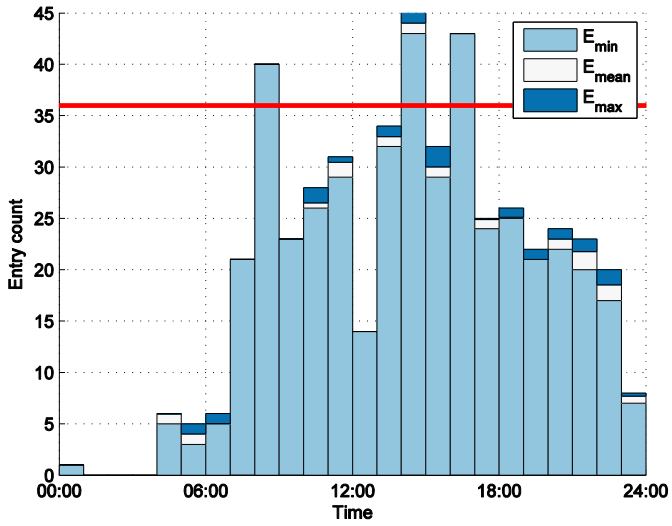

Figure 10. Entry count for $t_s = 60$ min and δt =60 min.

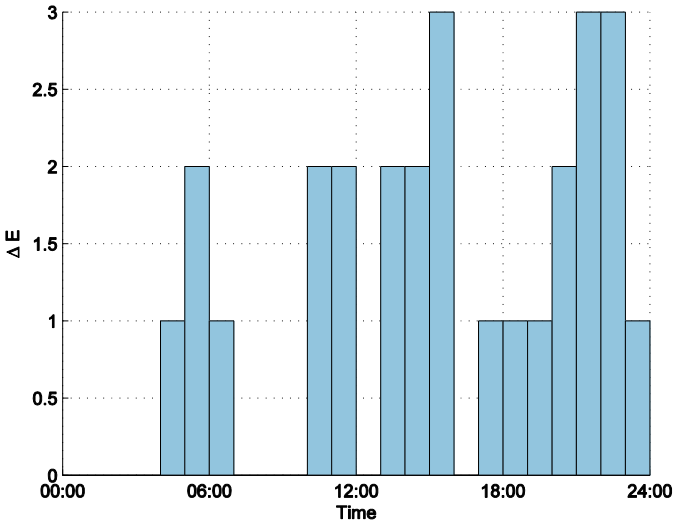

Figure 11. Dispersion of the entry count for $t_s = 60$ min and δt =60 min.

In Figure 12, the entry count is shown for shorter time periods, t_s =10 min and δt =10 min. Assuming that the capacity is 6 aircraft/10 minutes (one sixth of the declared capacity, 36 aircraft/hour), it is seen that this capacity is clearly exceeded multiple times.

When shortening the duration of the time period, the average values of the counts are proportionally reduced, but it can be seen that the dispersions are not, they remain with values around 2-3 aircraft; thus, the uncertainty is relatively more important. Now, the largest dispersion on the entry count is 4 flights (for 22:30-22:40 and 22:40-22:50). The dispersion of the entry count is shown in Figure 13; it can be observed that the dispersion is 4 flights for a total of 0.33 hours, 3 flights for 1.83 hours, 2 flights for 5.83 hours, 1 flight for 8 hours, and 0 flights for the remaining 8 hours.

DOI: 10.13009/EUCASS2017-263

If the duration of the time period is reduced to 1 minute, then the maximum dispersion is 5 flights for the entry count. Thus, as expected, the maximum value of dispersion increases as the duration of the time period decreases.

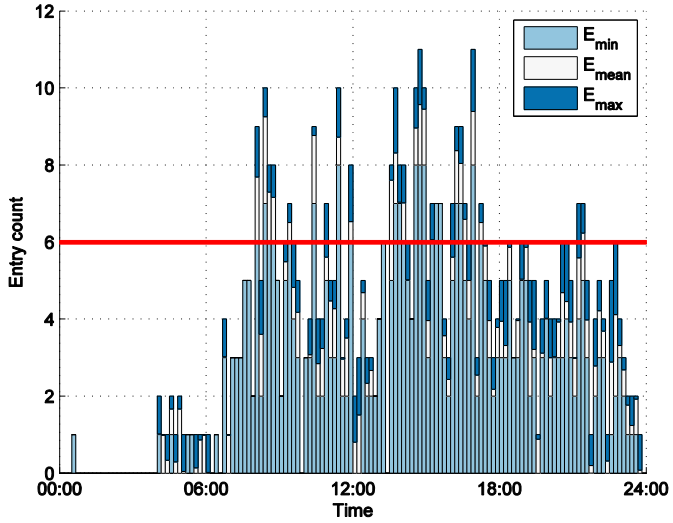

Figure 12. Entry count for t_s =10 min and δt =10 min.

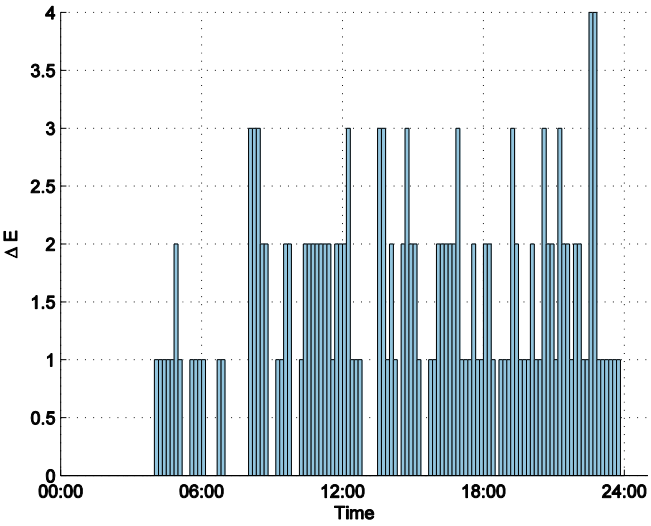

Figure 13. Dispersion of the entry count for t_s =10 min and δt = 10 min.

Probability of exceeding the declared capacity

The probability of the entry count being greater than the declared capacity (36 aircraft/hour) for t_s =60 min and δt =60 min is shown in Figure 14. This probability takes the value 1 for time periods 08:00-09:00, 14:00-15:00, and 16:00-17:00, and 0 otherwise. Therefore, there is a total assurance in having a capacity shortfall for these periods. Since the severity of the ATFCM measures depends on the value of the capacity shortfall, this deficit should be quantified. In this application, this maximum deficit is considered, measured as the difference between the maximum entry count and the declared capacity. It is marked by asterisks in Figure 14 (this maximum deficit can be easily identified in Figure 10 by the periods with higher maximum entry counts). It can be seen that the period 14:00-15:00 is the most severe, with a maximum deficit of 9 flights.

DOI: 10.13009/EUCASS2017-263

The probability of exceeding a capacity of 6 aircraft/10 minutes for $t_s = 10$ min and $\delta t = 10$ min is shown in Figure 15. In this case, intermediate values of probability are found. For example, if a probability threshold of 0.8 is considered, this value is exceeded in 18 different time periods, a total of 3 hours. In Figure 15, the capacity deficit is only shown for periods with a probability value above 0.8; the periods 14:40:14:50 and 16:50-17:00 are the most severe, with a maximum deficit of 5 flights.

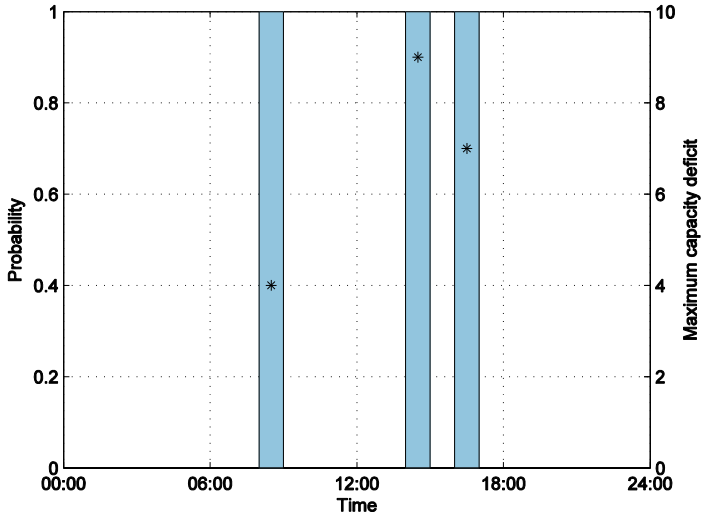

Figure 14. Probability of exceeding a capacity of 36 flights/hour (bars) and maximum capacity deficit (asterisks), for t_s =60 min and δt =60 min.

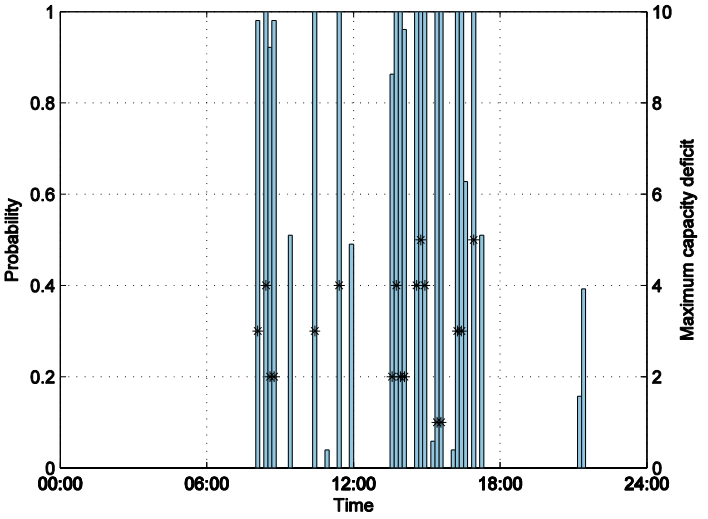

Figure 15. Probability of exceeding a capacity of 6 flights/hour (bars) and maximum capacity deficit (asterisks), for t_s =10 min and δt =10 min.

5. Final remarks

The methodology developed in the TBO-Met project to assess the uncertainty of sector demand when meteorological uncertainty is taken into account has been presented in this paper. This methodology requires to define a scenario in terms of Air Traffic Control sector, flights, and weather forecasts. In this work, the meteorological uncertainty is provided by Ensemble Weather Forecasting; in particular, by Ensemble Prediction Systems. A trajectory predictor computes, for each flight and for each possible atmosphere realization, a different aircraft trajectory. The computed trajectories along with the information of the sector, are then used to analyse the sector demand.

DOI: 10.13009/EUCASS2017-263

The analysis is based on the statistical characterization of the entry times of the flights to the sector, and of the entry count. Mean, maximum, and minimum values, and the spread of these times and this count are obtained. The probability of the count of exceeding given thresholds is also obtained, which can be used to represent the probability that the demand exceeds the declared capacity of the sector. This probability can be useful in the Demand-Capacity Balancing process. The higher the value of the probability and the capacity deficit, the more severe the Air Traffic Flow and Capacity Management measure to be considered.

The statistical characterization has been performed under certain general hypotheses. Two of them can be highlighted: the geometry of the sector is considered to be fixed over time, and the aircraft trajectories cross the sector only once. The opening and/or closing of sectors would result in transient effects, and the returning of aircraft to their departure airport is an uncommon practice. These two hypotheses do not impact the objective of this work: to help in the understanding of how weather uncertainty is propagated from the trajectory scale to the traffic scale.

A realistic application example has been provided in this paper to show the potentiality of the methodology. The demand of the ATC sector LECMSAU is analysed for a whole day when predicted the day before. The meteorological uncertainty is obtained from the ensemble forecast ECMWF-EPS. In this application, cruise flights at constant pressure altitude are assumed. A trajectory predictor that takes into account the uncertainty in wind and air temperature has been developed for this application.

In this particular example, it has been found that, because uncertainty is accumulated along the flight, the uncertainty in the entry times increases as the distance travelled by the aircraft to the entry point increases. Also, it has been found that the uncertainty in the entry count is large. For hourly entry counts, it is about 8%, when compared with the declared capacity of the sector, and larger values are found when smaller time periods are considered

This methodology can be extended to analyse the occupancy count, that is, the number of flights inside the sector during a selected time period. For this count, it is necessary to consider also the exit time from the sector, which is affected also by the weather uncertainties present inside the ATC sector.

In future works under the scope of TBO-Met project, this methodology will be applied to quantify the effects of weather uncertainty on convective phenomena (the uncertainty will be obtained from probabilistic nowcasts) and to quantify the benefits of improving the predictability of individual trajectories on the predictability of sector demand.

Acknowledgements

This work is part of the project TBO-Met. This project has received funding from the SESAR Joint Undertaking under grant agreement No 699294 under European Union’s Horizon 2020 research and innovation programme

References

[1] Rivas, D., and R. Vazquez. 2016. Uncertainty, in *Complexity Science in Air Traffic Management*, A. Cook and D. Rivas Ed., Ashgate Publishing Limited, Chap. 4.

[2] World Meteorological Organization. 2012. Guidelines on Ensemble Prediction Systems and Forecasting. WMO-No. 1091.

[3] Steiner, M., R. Bateman, D. Megenhardt, Y. Liu, M. Xu, M. Pocernich and J. A. Krozel. 2010. Translation of ensemble weather forecasts into probabilistic air traffic capacity impact. Air Traffic Control Quarterly, vol. 18, no. 3, pp. 229-254.

[4] Cheung, J., A. Hally, J. Heijstek, A. Marsman, and J.-L. Brenguier. 2015. Recommendations on trajectory selection in flight planning based on weather uncertainty. In: 5th SESAR Innovation Days (SID2015), pp. 1–8.

[5] Gonzalez-Arribas, D., M. Soler, and M. Sanjurjo. 2016. Wind-based robust trajectory optimization using meteorological ensemble probabilistic forecasts. In: 6th SESAR Innovation Days (SID2016), pp. 1–8.

[6] Franco, A., D. Rivas, and A. Valenzuela. 2017. Optimal Aircraft Path Planning Considering Wind Uncertainty. In: 7th European Conference for Aeronautics and Space Sciences (EUCASS), pp. 1-11.

[7] Dalichampt, M., and C. Plusquellec. 2007. Hourly Entry Count versus Occupancy Count – Definitions and indicators (I). EEC Note No. 15/07. Eurocontrol Experimental Centre.

[8] Nuic, A. 2015. User manual for the base of aircraft data (BADA), rev 3.13.